A computational study of the nonlinear optical properties of carbazole derivatives: Theory refines experiment

ARTICLE *in* THEORETICAL CHEMISTRY ACCOUNTS · JANUARY 2014

Impact Factor: 2.23 · DOI: 10.1007/s00214-014-1458-9

6 AUTHORS, INCLUDING:

Osman Abdelkarim
King Abdulaziz University
36 PUBLICATIONS **295** CITATIONS
SEE PROFILE

Nuha Wazzan
King Abdulaziz University
17 PUBLICATIONS **59** CITATIONS
SEE PROFILE

Abdullah M. Asiri
King Abdulaziz University
1,155 PUBLICATIONS **6,804** CITATIONS
SEE PROFILE

Theor Chem Acc (2014) 133:1458
DOI 10.1007/s00214-014-1458-9

REGULAR ARTICLE

A computational study of the nonlinear optical properties of carbazole derivatives: theory refines experiment

Alejandro J. Garza · Osman Ibrahim Osman · Nuha Ahmed Wazzan · Sher Bahadar Khan · Abdullah Mohamed Asiri · Gustavo E. Scuseria

Received: 2 December 2013 / Accepted: 30 January 2014 / Published online: 16 February 2014

Abstract The nonlinear optical (NLO) properties of *N*-ethyl dicyanocarbazole (**1**), *N*-ethyl cyanoethylacetatecarbazole (**2**), and *N*-ethyl dimethylacetatecarbazole (**3**) are studied with traditional hybrid and long-range corrected (LC) density functional theory (DFT) methods. The carbazoles are predicted to have planar structures with a high degree of π-conjugation and charge transfer, resulting in measurable NLO responses. The DFT data here calculated allow us to refine and correct previously reported experimental hyperpolarizabilities for these compounds. Experimental UV–vis absorption bands (related to hyperpolarizabilities estimated via solvatochromism) are also accurately reproduced by LC-DFT when using gap fitting schemes. The effects of different functionals on the HOMO–LUMO energy gaps and eventually on the total hyperpolarizabilities are discussed.

Keywords Hyperpolarizabilities · Organic materials DFT · Range separated hybrids · Solvatochromic method

A. J. Garza · G. E. Scuseria (✉)
Department of Chemistry, Rice University, Houston, TX 77251-1892, USA
e-mail: guscus@rice.edu

O. I. Osman · N. A. Wazzan · S. B. Khan · A. M. Asiri · G. E. Scuseria
Chemistry Department, Faculty of Science, King Abdulaziz University, Jidda 21589, Saudi Arabia

A. M. Asiri
Center of Excellence for Advanced Materials Research (CEAMR), King Abdulaziz University, Jidda 21589, Saudi Arabia

G. E. Scuseria
Department of Physics and Astronomy, Rice University, Houston, TX 77251-1892, USA

1 Introduction

The discovery of the change in the refractive index of a material due to an electric field by Kerr [1] in 1875, called the quadratic electro-optic effect, marked the birth of the nonlinear optical (NLO) field. Already in the 1950s, Hirshberg [2] proposed the use of NLO photochromic compounds for optical data storage. However, the widespread use of NLO effects was not enabled until the invention of lasers [3] in 1960 and the observation of second harmonic generation (SHG) in quartz a year later [4]. Since then, materials with large NLO susceptibilities have attracted much attention due to their possible applications in electro-optic and data-storage devices [5–11].

The link between molecular and NLO properties can be established by considering the interaction of an electric field **E** with the permanent dipole moment $\boldsymbol{\mu}$ of a molecule. Assuming the Taylor convention and summation over repeated indices, this effect may be expressed as [12]

$$\mu_i(\mathbf{E}) = \mu_i^0 + \alpha_{ij}E_j + \frac{1}{2!}\beta_{ijk}E_jE_k + \frac{1}{3!}\gamma_{ijkl}E_jE_kE_l + \cdots \quad (1)$$

where $\boldsymbol{\mu}^0$ is the dipole moment in the absence of the field, $\boldsymbol{\alpha}$ the polarizability, $\boldsymbol{\beta}$ the first-order hyperpolarizability, $\boldsymbol{\gamma}$ the second-order hyperpolarizability, and so on. Equation 1 implies that large tensor components β_{ijk} and γ_{ijkl} will lead to NLO behavior. Furthermore, in quantum chemistry, the molecular dipole moment can also be written in terms of the atomic charges Z_A, nuclear coordinates $\mathbf{R}_A$, basis $\{\chi\}$, and first-order reduced density matrix D_{ab} (or Kohn–Sham density matrix in DFT) as

$$\boldsymbol{\mu} = \sum_A Z_A\mathbf{R}_A - \sum_{ab} D_{ab}\langle\chi_a|\mathbf{r}|\chi_b\rangle. \quad (2)$$

Thus, standard methods of quantum chemistry can be used to compute hyperpolarizability tensors by differentiation of

the dipole moment with respect to the electric field [13–16].

In terms of accuracy and computational cost, the best option to calculate molecular hyperpolarizabilities of sizable molecules is long-range corrected (LC) DFT [17–22]. It is well established that widely used GGA and traditional hybrid functionals tend to overestimate NLO properties [23–27], whereas LC-DFT substantially improves the description of such phenomena [28–38]. Compounds with a low-lying, asymmetric, long-range charge-transfer resonance state display large β_{ijk} values [39–43]. One of the reasons for the LC-DFT success compared to traditional hybrids or GGAs is that LC functionals describe more appropriately these states because they incorporate a larger fraction of Hartree–Fock exchange as the interelectronic distance increases. That is, LC-DFT separates the exchange energy E_x in short and long-range (SR and LR) contributions

$$E_x^{\mathrm{LC-DFT}} = E_x^{\mathrm{SR-DFT}} + E_x^{\mathrm{LR-HF}}. \tag{3}$$

This division is in turn accomplished by splitting the interelectronic Coulomb operator r_{12}^{-1} as

$$\frac{1}{r_{12}} = \underbrace{\frac{1-\mathrm{erf}(\omega r_{12})}{r_{12}}}_{\mathrm{SR}} + \underbrace{\frac{\mathrm{erf}(\omega r_{12})}{r_{12}}}_{\mathrm{LR}} \tag{4}$$

where erf is the error function and ω a parameter defining the range separation.

In this work, we use LC-DFT to calculate optical and NLO properties of *N*-ethyl dicyanocarbazole (**1**), *N*-ethyl cyanoethylacetatecarbazole (**2**), and *N*-ethyl dimethylacetatecarbazole (**3**), whose structures are shown in Fig. 1. Our interest in these compounds originates from studies by Asiri et al. [44] that indicated that these molecules have large first-order hyperpolarizabilities arising from charge-transfer resonance states. However, the reported hyperpolarizabilities were obtained using the solvatochromic method [45–47], which is considered at best a rough estimate of the largest component of the hyperpolarizability

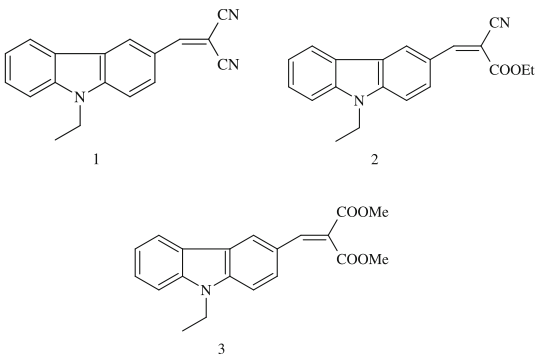

Fig. 1 Carbazole derivatives studied in this work

β_{zzz} [48]. The LC-DFT calculations carried out here confirm that these compounds are indeed charge-transfer NLO materials and allow us to refine and correct the β_{zzz} values reported in Ref. [44].

2 Methods

2.1 Hyperpolarizabilities

Because of the different conventions and methods used to measure hyperpolarizabilities, much confusion can arise when comparing experimental and theoretical data [48–50]. Hence, we dedicate this section to explain the conventions utilized here.

For the theoretical calculations, we employ as a measure of $\boldsymbol{\beta}$ the total hyperpolarizability β_{tot} given as

$$\beta_{\mathrm{tot}} = \sqrt{\beta_x^2 + \beta_y^2 + \beta_z^2} \tag{5}$$

where

$$\beta_i = \beta_{iii} + \frac{1}{3}\sum_{i\neq j}(\beta_{ijj} + \beta_{jij} + \beta_{jji}). \tag{6}$$

The β_{tot} reported here are frequency independent and the coordinate system is defined by the standard orientation of the molecules. Since experimentalists usually determine hyperpolarizabilities from SHG $\beta_{\parallel}(-2w;\ w,\ w)$ and the solvatochromic method $\beta_{zzz}(2w)$, we also report these quantities for some of the DFT calculations. These two are (theoretically) related by the equation $\beta_{zzz}(2w) = (5/3)\ \beta_{\parallel}(-2w;\ w,\ w)$. Note that the notation that we use indicates explicitly the frequency dependence of the hyperpolarizability by writing $\beta(2w)$. All these data are reported in atomic units (a.u.), which are related to the electrostatic units (esu) through the relation 1 a.u. $= 8.6393 \times 10^{-33}$ esu for β, and 1 a.u. $= 5.0367 \times 10^{-40}$ esu for γ.

The Taylor (T) convention [48, 49] (see also Eq. 1) for hyperpolarizabilities is used. We note, however, that β_{zzz} from solvatochromic measurements are often reported in the X (or phenomenological, since it absorbs numerical factors into the definition of polarizabilities) convention (see, e.g., Refs. [45, 47]). For hyperpolarizabilities, the T and *X* conventions are related by $\beta^T = 4\ \beta^X$ (for further details, see Ref. [48]).

2.2 Charge-transfer indices

As a quantitative measure of the spatial extent and magnitude of charge transfer in the carbazoles, we employ the indices proposed by Le Bahers et al. in Ref. [51]. Specifically, we compute q_{CT} and D_{CT}, which quantify the charge transferred in an excitation and its corresponding length.

These indices are calculated as follows: the functions $\rho_+(r)$ and $\rho_-(r)$ are defined as

$$\rho_+(r) = \begin{cases} \Delta\rho(r) & \text{if} \quad \Delta\rho(r) > 0 \\ 0 & \text{if} \quad \Delta\rho(r) < 0 \end{cases} \tag{7}$$

and

$$\rho_-(r) = \begin{cases} \Delta\rho(r) & \text{if} \quad \Delta\rho(r) < 0 \\ 0 & \text{if} \quad \Delta\rho(r) > 0, \end{cases} \tag{8}$$

where $\Delta\rho(r) = \rho_e(r) - \rho_g(r)$ is the difference in density between the excited and ground states. The barycenters of the spatial regions spanned by $\rho_+(r)$ and $\rho_-(r)$, R_+ and R_- are given by

$$R_\pm = \pm q_{CT}^{-1} \int r\rho_\pm(r)\mathrm{d}r \tag{9}$$

where the index q_{CT} is

$$q_{CT} = \int \rho_+(r)\mathrm{d}r = -\int \rho_-(r)\mathrm{d}r, \tag{10}$$

and D_{CT} is the distance between the barycenters

$$D_{CT} = |R_+ - R_-|. \tag{11}$$

The total variation in the dipole moment for the excitation μ_{CT} is calculated straightforwardly from q_{CT} and D_{CT} as $\mu_{CT} = q_{CT}\ D_{CT}$. A more thoroughly explanation of these indices is, of course, available in the original paper [51].

2.3 Computational details

All calculations were carried using the Gaussian 09 suite of programs [52]. A modified version of this code was used to compute hyperpolarizabilities using the LC-ωPBE functional and the q_{CT} and D_{CT} indices. The LC-DFT functionals used in this work are CAM-B3LYP, ωB97XD, and LC-ωPBE. As in Ref. [51], the 6-31+G(d) basis was employed to calculate q_{CT} and D_{CT}. The 6-311++G(d,p) and 6-311+G(d,p) basis sets were utilized for the rest of the calculations; these have been shown to be more than adequate for computing NLO properties of neutral molecules with DFT [53]. Indeed, Suponitsky et al. [53] showed that, while a set of diffuse functions is essential for quantitative calculations of β, using basis sets more complete than 6-31+G(d) results in very small changes in hyperpolarizability. The geometries of **1**, **2**, and **3** were fully optimized at the indicated level of theory with standard thresholds defined by Gaussian's `Opt` keyword. Likewise, default parameters given by the `Polar` keyword are used in the computation of hyperpolarizabilities (this implies the analytical computation of these quantities). Similar calculations using the B3LYP functional were also carried out for comparison purposes.

Frequency dependent $\beta_\parallel(-2w; w, w)$ at a wavelength of 1,064 nm (commonly used in SHG experiments), and time-dependent DFT excited states were also computed at the LC-ωPBE/6-311+G(d,p) level. The densities of the ground and first excited states were analyzed using Gaussview [54] to characterize the charge-transfer nature of the states. For comparison with experiment, some of these calculations were done in solvent media; these calculations were performed using the polarizable continuum model (PCM) to mimic solvent effects [55]. Default options of the `SCRF` keyword were used for these simulations. As a reference point, we also show data for *p*-nitroaniline (pNA) because this molecule is the canonical example of a charge-transfer species with high hyperpolarizability, and as a such, there is a substantial amount of experimental and theoretical data of high quality for this compound [56, 57].

3 Results and discussion

3.1 Geometries and hyperpolarizabilities

The geometry optimizations with the different DFT methods gave all bonds and angles typical of sp^2, π-conjugated systems. Also, since the molecules differ only by the substituents, the carbazole rings in **1**, **2**, and **3** share all a similar geometry. However, while **1** and **2** are completely planar, there is some deviation from planarity in the CO-OMe groups of **3**. This seems to arise from steric interactions between the more bulky pair of COOMe groups, and it also appears to break the conjugation to some degree resulting in a lower β_{tot} for **3** as compared to **1** and **2** (see Table 1).

Table 1 lists the calculated dipole moments, the total hyperpolarizabilities, and the HOMO–LUMO gaps (E.G.) for **1**, **2**, **3**, and pNA. It is seen in comparison with the pNA data that all three carbazoles have measurable NLO properties ($\sim \times 3 - 4\beta$ of pNA), with **1** and **2** having the largest hyperpolarizabilities. These two chromophores also have a larger dipole moment than **3**, pointing toward a greater charge separation in the former. This larger charge separation is quantified by the indices listed in Table 2; while q_{CT} is calculated equal to 0.5 a.u. for all three carbazoles, the length of the charge-transfer excitation D_{CT} is smaller for **3** than for **1** or **2**, correlating with the dipole moments and hyperpolarizabilities. Also, due to delocalization, D_{CT} is shorter than the distance between the donor and acceptor groups, in agreement with the observations in Ref. [51]. A visual representation of the charge variations during the excitation is given in Fig. 2, which depicts a map of the difference in total electronic density between the ground and first excited states computed by time-dependent LC-ωPBE; the long-range charge-transfer nature of the states is

evident in these maps. Hence, the DFT calculations confirm the experimental evidence in Ref. [44] of **1**, **2**, and **3** being donor–acceptor chromophores with large hyperpolarizabilities arising from charge transfer.

Table 1 Gas-phase dipole moments (μ/Debye), total hyperpolarizabilities (β_{tot}/a.u.), HOMO–LUMO energy gaps (E.G./eV), and second harmonic generation hyperpolarizabilities ($\beta_{\|}(-2w;w,w)$/a.u. at $w = 1{,}064$ nm)

Method	Parameter	1	2	3	pNA
B3LYP/6-311++G(d,p)	μ	10.3	8.9	4.2	7.5
	β_{tot}	5,006	5,814	4,622	1,651
	E.G.	3.52	3.57	3.93	4.16
CAM-B3LYP/6-311++G(d,p)	μ	9.8	8.6	4.1	7.2
	β_{tot}	4,261	4,633	3,326	1,361
	E.G.	5.89	5.98	6.41	6.82
ωB97XD/6-311++G(d,p)	μ	9.9	8.5	6.0	7.1
	β_{tot}	4,247	4,381	2,753	1,273
	E.G.	6.93	7.06	7.53	8.01
LC-ωPBE/6-311+G(d,p)	μ	9.4	6.6	4.7	6.9
	β_{tot}	3,865	3,873	2,426	1,118
	E.G.	7.96	8.07	8.03	9.14
	$\beta_{\|}(-2w;w,w)$	4,038	4,084	2,380	985
Experiment	μ	–	–	–	6.9
	$\beta_{\|}(-2w;w,w)$	–	–	–	1,072 ± 44

Data for *p*-nitroaniline (pNA) is also given for comparison purposes; the experimental data for this compound were taken from Refs. [56, 57]

Table 2 Distance between donor and acceptor groups $d(N_D - B_A)$ (Å) and calculated charge-transfer indices D_{CT} (Å), q_{CT} (a.u.), and μ_{CT} (Debye) for the carbazoles at the LC-ωPBE/6-31+G(d) level with LC-ωPBE/6-311+G(d,p) geometries

Molecule	$d(N_D - B_A)$	D_{CT}	q_{CT}	μ_{CT}
1	6.62	2.6	0.5	6.4
2	6.72	2.5	0.5	6.0
3	6.64	2.2	0.5	5.3

An inverse relationship between HOMO–LUMO energy gaps has been previously pointed out for carbazoles [44] and fluorenyl derivatives [58]. Although the physical meaning of the Kohn–Sham orbitals in DFT is a matter of debate [59–62], we see here that the hyperpolarizabilities can be arranged in order of magnitude B3LYP > CAM-B3LYP > ωB97XD > LC-ωPBE, and that this order is inverted for E.G. values. Analogous observations for other chromophores have been reported in Refs. [63, 64]. Thus, although the Kohn–Sham orbital energies do not need to correspond to those of true molecular orbitals, there still seems to be an inverse relationship between the β and E.G. values computed by DFT functionals for several donor–acceptor molecules. This relationship could perhaps be explained considering the formalism of the ΔSCF method [65], where an actual orbital excitation of the Kohn–Sham determinant is considered to simulate excited states. Therefore, an actual relationship between the Kohn–Sham E.G. value and the true energy difference between the ground and excited state could be expected. A lower E.G. value would then lead to a higher β in donor–acceptor chromophores due to the lower energy threshold for charge transfer.

3.2 Comparison with solvatochromic measurements

The hyperpolarizabilities estimated in Ref. [44] by the solvatochromic method are more than ten times greater than those in Table 1. Moreover, noting that the formulae in the *X* convention given by Song [47] were used in that reference, the β values given there would need to be multiplied by four in order to compare with our results here, further increasing the discrepancy. This huge disagreement prompted us to recalculate the values for β_{zzz} from the data in Ref. [44], and to question the applicability of the solvatochromic method for the carbazole derivatives in question. For the sake of clarity, a description of the method is germane here.

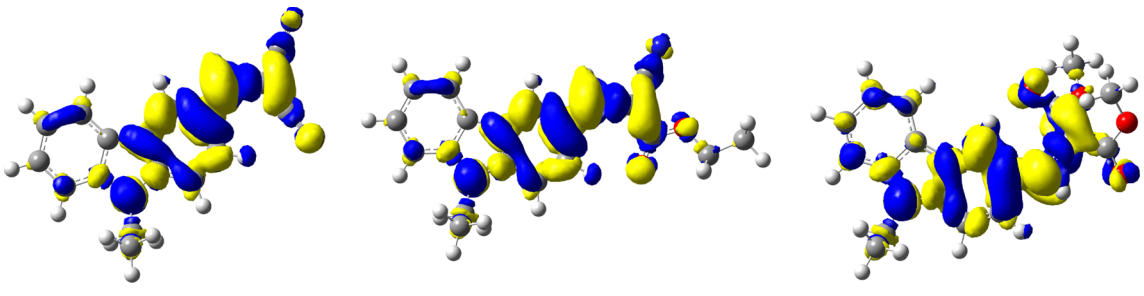

Fig. 2 Difference in total electronic density (isocontour value of 0.001 a.u.) between the ground and first excited states of **1**, **2**, and **3** at the LC-ωPBE/6-311+G(d,p) level. *Yellow* (*blue*) regions indicate a gain (loss) of density in the excited state

The solvatochromic method is based on a two-state approximation to the largest β_{ijk} component β_{zzz}. At a frequency w, β_{zzz} $(2w)$ is estimated by [45–48]

$$\beta_{zzz}(2w) = \frac{1}{(1 - w^2/w_{eg}^2)(1 - 4w^2/w_{eg}^2)}\beta_0, \tag{12}$$

$$\beta_0 = \frac{6\mu_{eg,z}^2(\mu_{e,z} - \mu_{g,z})}{w_{eg}^2}, \tag{13}$$

where $\mu_{eg,z} = \langle \Psi_e | \hat{\mu_z} | \Psi_g \rangle$, $\mu_{e,z}$ and $\mu_{g,z}$ are transition and dipole moments (in a.u.) for the excited and ground states in the z direction, and w_{eg} is the transition frequency $|\Psi_g\rangle \rightarrow |\Psi_e\rangle$ (in Hartrees). The quantities appearing in the equations above can be extracted from spectroscopic data; w_{eg} is simply the band maximum of the UV–vis absorption spectrum, whereas $\mu_{eg,z}$ can be obtained from the area under the band A by the relation [45, 47]

$$A = \frac{2w_{eg}N_A n \mu_{eg,z} M}{3(2.303)c} \tag{14}$$

where N_A is Avogadro's number, n the refraction index, M the solute concentration, and c the speed of light in vacuum. Lastly, solvatochromism is used to estimate $\mu_{e,z}$ and $\mu_{g,z}$ from spectral data in various solvents. This technique requires the measurement of Stokes shifts $(w_a - w_f)$ and usually employs Lippert's equation [66, 67]

$$w_a - w_f = mf(\epsilon, n) + \text{constant}, \tag{15}$$

or the Bakshiev's and Kawski–Chamma–Viallet's equations [68–72]

$$w_a - w_f = m_1 f_1(\epsilon, n) + \text{constant} \tag{16}$$

$$\frac{w_a + w_f}{2} = -m_3 f_2(\epsilon, n) + \text{constant} \tag{17}$$

with ϵ = dielectric constant of solvent, and

$$f(\epsilon, n) = \frac{\epsilon - 1}{2\epsilon + 1} - \frac{n^2 - 1}{2n^2 + 1}, \tag{18}$$

$$f_1(\epsilon, n) = \frac{2n^2 + 1}{n^2 + 2}\left(\frac{\epsilon - 1}{\epsilon + 2} - \frac{n^2 - 1}{n^2 + 2}\right), \tag{19}$$

$$f_2(\epsilon, n) = \frac{1}{2}f_1(\epsilon, n) + \frac{3}{2}\frac{n^4 - 1}{n^2 - 1}, \tag{20}$$

$$m = m_1 = \frac{2(\mu_{e,z} - \mu_{g,z})^2}{a^3}, \tag{21}$$

$$m_2 = \frac{2(\mu_{e,z}^2 - \mu_{g,z}^2)}{a^3} \tag{22}$$

where a is the Onsager radius of the molecule. Hence, one can use Stokes shifts in different solvents to solve for m in Eq. 15, or m_1 and m_2 in Eqs. 16 and 17. To get the dipole moments from m or m_1 and m_2, the value of a is estimated to be 0.7 times the molecular length; this choice is somewhat arbitrary but often used in the absence of a clear better option.

Table 3 Values for the frequencies (in Hartrees) w_{eg}, w_a, w_f and solvent polarity functions (dimensionless)

Molecule	Parameter	Chloroform	Acetonitrile
1	$w_{eg} = w_a$	0.1093	0.1119
	w_f	0.0881	0.0904
2	$w_{eg} = w_a$	0.1131	0.0878
	w_f	0.1151	0.0934
3	$w_{eg} = w_a$	0.1360	0.1385
	w_f	0.1070	0.1090
1, **2**, **3**	$f(\epsilon, n)$	0.1480	0.3054
1, **2**, **3**	$f_1(\epsilon, n)$	0.3701	0.8630
1, **2**, **3**	$f_2(\epsilon, n)$	0.4871	0.6658

The frequencies were taken from UV–vis and fluorescence spectra in Ref. [44]

Table 4 Values for $\mu_{eg,z}$, $\Delta\mu_{eg,z}$, and $\beta_{zzz}(2w)$ (in $CHCl_3$) computed by the solvatochromic method (using data from Ref. [44]) and PCM-LC-ωPBE/6-311+G(d,p)

Molecule	Parameter	Solvatochromism	LC-ωPBE
1	$\mu_{eg,z}$	2.6	3.0
	$(\mu_{e,z} - \mu_{g,z})$	2.1[a], 1.2[b]	2.6
	$\beta_{zzz}(2w)$	21,776[a], 12,547[b]	14,044
2	$\mu_{eg,z}$	2.8	3.1
	$(\mu_{e,z} - \mu_{g,z})$	NA[c]	3.0
	$\beta_{zzz}(2w)$	30,200[d]	8,425
3	$\mu_{eg,z}$	2.0	2.2
	$(\mu_{e,z} - \mu_{g,z})$	2.2[a], 1.3[b]	2.1
	$\beta_{zzz}(2w)$	5,254[a], 3,104[b]	5,613

All values are reported in atomic units

[a] Eq. 15

[b] Eqs. 16 and 17

[c] Solvatochromic equations yield imaginary values

[d] Estimated with $\Delta\mu_{eg,z}$ from LC-ωPBE

With these formulae, we can now calculate β_{zzz} $(2w)$ using the data from Ref. [44]. The values of a were estimated (from the gas-phase geometries) to be 15.0, 19.3, and 15.4 bohr for **1**, **2**, and **3**, respectively. For convenience, the spectroscopic data from Ref. [44] required for the calculations are listed in Table 3; the laser frequency is w = 1,064 nm = 0.0428 Hartree. The solvatochromic dipole moment and hyperpolarizabilities computed with these data are given in Table 4 and compared with results from PCM-LC-ωPBE/6-311+G(d,p) calculations in chloroform.

The frequency dependent PCM–DFT hyperpolarizabilities are larger than those in gas phase (Table 1) because of solvent effects and resonant enhancement (which is

reflected in the prefactor to β_0 in Eq. 12). The experimental and theoretical $\mu_{eg,z}$ values in Table 4 are in fair agreement among each other. However, it is evident from this table that the solvatochromic method cannot provide accurate estimates of the hyperpolarizabilities of the carbazoles, depending on the approximation for the polarity functions (e.g., $f(\epsilon, n)$), values of β_{zzz} $(2w)$ can differ by large factors ($\sim$100 %). Moreover, $(\mu_{e,z} - \mu_{g,z})$ is calculated to be imaginary for **2** with this method, no matter which polarity function is used. Also, although the $(\mu_{e,z} - \mu_{g,z})$ values of **1** and **3** seem reasonable, the individual dipole moments $\mu_{e,z}$ and $\mu_{g,z}$ become negative when solving Eqs.16 and 17. These unphysicalities arise because of the many assumptions of the solvatochromic equations including (1) that there are no specific solvent–solute interactions, and (2) that the dipole moments of the ground and excited states are collinear. In fact, the TDDFT calculations suggest that this last assumption is not valid for **2**, possibly explaining the imaginary value of $(\mu_{e,z} - \mu_{g,z})$.

We note, however, that only two different solvents (chloroform and acetonitrile) are being used here to solve the solvatochromic equations. This approach is minimalistic and it is possible that, by making a least squares fit to m or m_1 and m_2 in a wide range of solvents, better results be obtained. Nevertheless, Reis [48] noted that previous solvatochromic measurements could claim a reasonable agreement with more accurate methods only because of (fortuitous) mistakes in not making the appropriate corrections for the hyperpolarizability conventions being used. The conclusion in that work was that the solvatochromic method yields at best a rough estimate of β_{zzz}, which is in accordance with our observations here.

3.3 UV–vis absorption bands

The prediction of UV–vis absorption maxima λ_{max} is useful for the characterization of NLO materials and their properties (e.g., photochromism or β_{zzz} by the solvatochromic method outlined above). Thus, we use here time-dependent LC-DFT to estimate λ_{max} for the carbazoles of interest, which may be considered as prototypes for other possible NLO carbazole derivatives.

Using LC-ωPBE with default parameters ($\omega = 0.4$ bohr^{-1}) yields the qualitatively correct ordering of wavelengths as $\lambda_{max}(\mathbf{1}) > \lambda_{max}(\mathbf{2}) > \lambda_{max}(\mathbf{3})$. However, the wavelengths are consistently underestimated and far off from their corresponding experimental values with errors up to about 100 nm (see Table 5). Indeed, studies involving a wide variety of organic dyes by Jacquemin et al. [30] report a mean average error of 72 nm in absorption bands for LC-ωPBE. Thus, this method does not seem reliable for giving quantitative results for absorption bands of chromophores.

Table 5 Values for ω (bohr^{-1}), $J_{gap}(\omega)$ (Hartree), as well as the corresponding absorption maxima (nm) in chloroform given by LC-ωPBE/6-311+G(d,p) compared to experiment (from Ref. [44])

Molecule	ω	$J_{gap}(\omega)$	$\lambda_{max}^{\text{LC-}\omega\text{PBE}}$	Error
1	0.4	0.97	321	−96
2	0.4	0.95	296	−107
3	0.4	0.92	292	−43
1	0.1	0.83	419	2
2	0.1	0.80	400	−3
3	0.1	0.77	374	39

The error (in nm) is given by theory–experiment

A simple and nonempirical way to improve these results is to use gap fitting schemes that tune the ω parameter so that the HOMO energy matches the first ionization potential [73–76]. That is, to choose ω so that it minimizes the function

$$J_{\text{gap}}(\omega) = J_{IP}(\omega) + J_{EA}(\omega) \tag{23}$$

with

$$J_{\text{IP}}(\omega) = \left|\epsilon_H^{\omega}(N) + E_{\omega}(N-1) - E_{\omega}(N)\right|, \tag{24}$$

$$J_{\text{EA}}(\omega) = \left|\epsilon_H^{\omega}(N+1) + E_{\omega}(N) - E_{\omega}(N+1)\right| \tag{25}$$

where ϵ_H^{ω} is the energy of the HOMO and E_{ω} (N) the total energy for the N-electron system. This scheme has been utilized by Karolewski et al. [75] and Pandey et al. [76] and has been shown to greatly improve the prediction of absorption spectra by LC-DFT. We also emphasize that this is a nonempirical correction because minimizing J_{gap} can be considered as an exact constraint that the functional must fulfill.

Here we take a minimalist approach and select the ω value that yields the lowest J_{gap} among the set $\omega = 0.1$, 0.2, 0.3, 0.4, and 0.5 bohr^{-1}. For all the three carbazoles, $\omega = 0.1$ bohr^{-1} gave the lowest J_{gap} values. The resulting λ_{max} values are in much better agreement with experiment (see Table 5); the average error for the three carbazoles is only about 15 nm, with errors of only $\sim$2–3 nm for **1** and **2**. The difference between the theoretical and experimental values of λ_{max} can be attributed in part due to the lack of vibrational and geometrical relaxation terms in the calculations. Hence, using a gap fitting scheme seems like a good option to compute UV–vis spectroscopic data of carbazoles when using LC-DFT.

4 Conclusions

We have applied LC-DFT, along with a variety of techniques, to compute the geometries, hyperpolarizabilities,

and other characteristics of the NLO properties of carbazoles **1**, **2**, and **3**. The LC-DFT calculations have proved reliable (here and in other works) for predicting hyperpolarizabilities in charge-transfer compounds, and have allowed us to refine and correct the experimental hyperpolarizability values of **1**, **2**, and **3** previously reported in the literature. The NLO behavior and charge-transfer nature of the carbazoles is confirmed by the DFT calculations. Furthermore, the fact that theory and computations can refine experimental measurements demonstrates the importance and usefulness of combining them in the study of NLO materials. The experimental UV–visible λ_{max} values of the carbazoles are also well reproduced (average error of $\sim$15 nm) by LC-DFT using a simple gap fitting scheme. Since compounds **1**, **2**, and **3** can be considered as prototype donor–acceptor carbazoles, LC-DFT methods seem to be an overall good choice for predicting optical and NLO properties of carbazole derivatives.

Acknowledgments This work was funded by King Abdulaziz University, under Grant No. (21-3-1432/HiCi). The authors, therefore, acknowledge technical and financial support of KAU.

References

1. Weinberger P (2008) Philos Mag Lett 88:897
2. Hirshberg Y (1956) J Am Chem Soc 78:2304
3. Maiman TH (1960) Nature 187:439
4. Franken PA, Hill AE, Peters CW, Weinreich G (1961) Phys Rev Lett 7:118
5. Marder SR, Sohn JE, Stucky GD (1991) Materials for non-linear optics: chemical perspectives, ACS symposium series 45, Washington, DC
6. Boyd RW (1992) Nonlinear optics. Academic Press, New York
7. Marder SR (2006) Chem Commun 2:131
8. Irie M (2000) Chem Rev 100:1685
9. Kawata S, Kawata Y (2000) Chem Rev 100:1777
10. Tian H, Yang S (2004) Chem Soc Rev 33:85
11. Dvornikov AS, Walker EP, Rentzepis PM (2009) J Phys Chem A 113:13633
12. Sekino H, Bartlett RJ (1993) J Chem Phys 98:3022
13. Norman P, Ruud K (2006) Microscopic theory of nonlinear optics. In: Papadopoulos MG, Sadlej AJ, Leszczynski J (eds) Nonlinear optical properties of matter: from molecules to condensed phases. Springer, The Netherlands
14. Cramer CJ (2004) Essentials of computational chemistry, 2nd edn. Wiley, England
15. Bishop DM, Kirtman B (1991) J Chem Phys 95:2646
16. Brédas JL, Adant C, Tackx P, Persoons A, Pierce BM (1994) Chem Rev 94:243
17. Savin A, Flad H (1995) Int J Quantum Chem 56:327
18. Iikura H, Tsuneda T, Yanai T, Hirao K (2001) J Chem Phys 115:3540
19. Yanai T, Tew DP, Handy NC (2004) Chem Phys Lett 393:51
20. Vydrov OA, Heyd J, Krukau AV, Scuseria GE (2006) J Chem Phys 125:074106
21. Vydrov OA, Scuseria GE (2006) J Chem Phys. 125:234109
22. Jacquemin D, Perpète EA, Vydrov OA, Scuseria GE, Adamo C (2007) J Chem Phys 127:094102
23. Champagne B, Perpete EA, van Gisbergen SJA, Baerends EJ, Snijders JG, Soubra-Ghaoui C, Robins KA, Kirtman B (1998) J Chem Phys 109:10489
24. Champagne B, Perpete EA, Jacquemin D, van Gisbergen SJA, Baerends EJ, Soubra-Ghaoui C, Robins KA, Kirtman B (2000) J Chem Phys 104:4755
25. Loboda O, Zaleśny R, Avramopoulos A, Luis JM, Kirtman B, Tagmatarchis N, Reis H, Papadopoulos MG (2009) J Phys Chem A 113:1159
26. van Faassen M, de van BoeijR. Leeuwen PL, Berger JA, Snijders JG (2003) J. Chem. Phys. 118:1044
27. Kirtman B, Lacivita V, Dovesi R, Reis H (2011) J Chem Phys 135:154101
28. Tawada Y, Tsuneda T, Yanagisawa S, Yanai T, Hirao K (2004) J Chem Phys 120:8425
29. Kamiya M, Sekino H, Tsuneda T, Hirao K (2005) J Chem Phys 122:234111
30. Jacquemin D, Perpète EA, Scuseria GE, Ciofini I, Adamo C (2008) J Chem Theory Comput 4:123
31. Perpète EA, Jacquemin D, Adamo C, Scuseria GE (2008) Chem Phys Lett 456:101
32. Jacquemin D, Perpète EA, Scuseria GE, Ciofini I, Adamo C (2008) Chem Phys Lett 465:226
33. Song J, Watson MA, Sekino H, Hirao K (2008) J Chem Phys 129:024117
34. Zaleśny R, Bulik IW, Bartkowiak W, Luis JM, Avramopoulos A, Papadopoulos MG, Krawczyk P (2010) J Chem Phys 133:244308
35. de Wergifosse M, Champagne B (2011) J Chem Phys 134:074113
36. Jacquemin D, Perpète EA, Medved M, Scalmani G, Frisch MJ, Kobayashi R, Adamo C (2007) J Chem Phys 126:191108
37. Nguyen KA, Rogers JE, Slagle JE, Day PN, Kannan R, Tan L, Fleitz PA, Pachter R (2006) J Phys Chem A 110:13172
38. Garza AJ, Scuseria GE, Khan SB, Asiri AM (2013) Chem Phys Lett 575:122
39. Oudar JL, Chemla DS (1977) J Chem Phys 66:2664
40. Hurst M, Munn RW (1989) Theory of molecular opto-electronics. VI. Comparison between nitroanilines. In: Hann RA, Bloor D (eds) Organic materials for nonlinear optics. The Royal Society of Chemistry, London
41. Kanis DR, Ratner MA, Marks TJ (1994) Chem Rev 94:195
42. Ramakrishna G, Goodson T III (2007) J Phys Chem A 111:993
43. Chakrabarti S, Ruud K (2009) Phys Chem Chem Phys 11:2592
44. Asiri AM, Khan SA, Al-Amoudi MS, Alamry KA (2012) Bull Korean Chem Soc 33(6):1900
45. Paley MS, Harris JM (1989) J Org Chem 54:3774
46. Deguan L, Ratner MA (1988) J Am Chem Soc 110:1707
47. Song H, Chem Y, Zheng X, Ying B (2001) Spectrochim Acta Part A 57:1717
48. Reis H (2006) J Chem Phys 125:014506
49. Willets A, Rice JE, Burland DM, Shelton D (1992) J Chem Phys 97:7590
50. Stäehlin M, Moylan CR, Burland DM, Willets A, Rice JE, Shelton DP, Donley EA (1993) J Chem Phys 98:5595
51. Le Bahers T, Adamo C, Ciofini I (2011) J Chem Theory Comput 7:2498
52. Frisch MJ, Trucks GW, Schlegel HB et al (2009) Gaussian 09, revision A.02. Gaussian Inc., Wallingford
53. Suponitsky KY, Tafur S, Masunov AE (2008) J Chem Phys 129:044109
54. Dennington R, Keith T, Millam J (2009) GaussView, version 5. Semichem Inc., Shawnee Mission KS
55. Tomasi J, Mennucci B, Cammi R (2005) Chem Rev 105:2999
56. Kaatz P, Donley EA, Shelton DP (1997) J Chem Phys 108:849
57. Sim F, Chin S, Dupuis M, Rice JE (1993) J Phys Chem 97:1158
58. Thanthiriwatte KS, Nalinde Silva KM (2002) Theochem 617:169

59. Perdew JP, Parr RG, Levy M, Balduz JL (1982) Phys Rev Lett 49:1691
60. Kleinman L (1997) Phys Rev B 56:12042
61. Perdew JP, Levy M (1997) Phys Rev B 56:16021
62. Kleinman L (1997) Phys Rev B 56:16029
63. Garza AJ, Osman OI, Scuseria GE, Wazzan NA, Khan SB, Asiri AM (2013) Theor Chem Acc 132:1384
64. Garza AJ, Osman OI, Scuseria GE, Wazzan NA, Khan SB, Asiri AM (2013) Comp Theor Chem 1022:82
65. Terranova U, Bowler DR (2013) J Chem Theory Comput 9:3181
66. Lippert E (1955) Z Naturforsch 10:541
67. Siddlingeshwar B, Hanagodimath SM (2009) Spectrochim Acta Part A Mol Biomol Spectrosc 72:490
68. Bakhshiev NG (1964) Opt Spektrosk 16:821
69. Kawski A, Bilot L (1964) Acta Phys Pol 26:41
70. Kawski A (1966) Acta Phys Pol 29:507
71. Chamma A, Viallet P (1970) CR Acad Sci Paris Ser C 270:1901
72. Raikar US, Renuka CG, Nadaf YF, Mulimani BG, Karguppikar AM, Soudagar MK (2006) Spectrochim Acta Part A Mol Biomol Spectrosc 65:673
73. Stein T, Kronik L, Baer R (2009) J Am Chem Soc 131:2818
74. Stein T, Kronik L, Baer R (2009) J Chem Phys 131:244119
75. Karolewski A, Stein T, Kümmel S (2011) J Chem Phys 134:151101
76. Pandey L, Doiron C, Sears JS, Brédas J (2012) Phys Chem Chem Phys 14:14243